Classification of wave regimes in excitable systems with linear cross diffusion

M. A. Tsyganov
Institute of Theoretical and Experimental Biophysics, Pushchino, Moscow Region, 142290, Russia

V. N. Biktashev
College of Engineering, Mathematics and Physical Sciences, University of Exeter, Exeter EX4 4QF, UK

(Received 4 July 2014; published 12 December 2014)

We consider principal properties of various wave regimes in two selected excitable systems with linear cross diffusion in one spatial dimension observed at different parameter values. This includes fixed-shape propagating waves, envelope waves, multienvelope waves, and intermediate regimes appearing as waves propagating at a fixed shape most of the time but undergoing restructuring from time to time. Depending on parameters, most of these regimes can be with and without the "quasisoliton" property of reflection of boundaries and penetration through each other. We also present some examples of the behavior of envelope quasisolitons in two spatial dimensions.

DOI: 10.1103/PhysRevE.90.062912 PACS number(s): 82.40.Bj, 82.40.Ck, 87.10.−e

I. INTRODUCTION

Progress in the study of self-organization phenomena in physical, chemical, and biological systems is dependent on study of generation, propagation, and interaction of nonlinear waves in spatially distributed active, e.g., excitable, systems with diffusion [1]. An important general property of such systems is their ability to generate and conduct self-supported strongly nonlinear waves of the change of state of the medium. The shape and speed of such waves in the established regime does not depend on initial and boundary conditions and is fully determined by the medium parameters. Until recently the results concerning such systems have been focused on systems "reaction + diffusion" with a diagonal diffusivity matrix, e.g., for two reacting components,

$$\frac{\partial u}{\partial t} = f(u,v) + D_u\nabla^2 u, \quad \frac{\partial v}{\partial t} = g(u,v) + D_v\nabla^2 v, \qquad (1)$$

with nonnegative diffusivities $D_u \geqslant 0, D_v \geqslant 0, D_u + D_v > 0$. However, a number of applications motivate consideration of a more generic class of reaction-diffusion systems, with nondiagonal elements of the diffusivity matrix ("cross diffusion"), which can produce a number of unusual patterns and wave regimes; see e.g., for a review Ref. [2]. In this paper we concentrate on one subclass of such unusual wave regimes, which is associated with soliton-like interaction, i.e., penetration of waves upon impact with each other or reflection from nonflux boundaries. This is rather uncharacteristic of the waves in (1) with the exception of narrow parametric regions on the margins of the excitability [3]. However, in systems with cross diffusion, such "quasisoliton" behavior can be observed in large parametric regions [4,5]. These phenomena have been observed in numerical simulations of two-component excitable media with cross diffusion, both in linear formulation, e.g.,

$$\begin{aligned}\frac{\partial u}{\partial t} &= f(u,v) + D_u\nabla^2 u + h_1\nabla^2 v,\\ \frac{\partial v}{\partial t} &= g(u,v) + D_v\nabla^2 v - h_2\nabla^2 u,\end{aligned} \qquad (2)$$

and in nonlinear, "taxis" formulation,

$$\begin{aligned}\frac{\partial u}{\partial t} &= f(u,v) + D_u\nabla^2 u + h_1\nabla(u\nabla v),\\ \frac{\partial v}{\partial t} &= g(u,v) + D_v\nabla^2 v - h_2\nabla(v\nabla u),\end{aligned} \qquad (3)$$

where $h_1 \geqslant 0, h_2 \geqslant 0, h_1 + h_2 > 0$.

Quasisolitons have similarities and differences with the classical solitons in conservative (fully integrable) systems. The already mentioned similarity is their ability to penetrate through each other and reflect from boundaries. The differences are the following:

(1) The amplitude and speed of a true soliton depend on initial conditions. For the quasisoliton, the established amplitude and speed depend on the medium parameters.

(2) The amplitudes of the true solitons do not change after the impact. The dynamics of quasisolitons on impact is often naturally seen as a temporary diminution of the amplitude with subsequent gradual recovery.

Recently we have demonstrated "envelope quasisolitons" in one-dimensional systems with linear cross diffusion (2) [6], which share some phenomenology with envelope solitons in the nonlinear Schrödinger equation (NLS) for a complex field w [7],

$$i\frac{\partial w}{\partial t} + \nabla^2 w + w|w|^2 = 0. \qquad (4)$$

Namely, they have the form of spatiotemporal oscillations ("wavelets") with a smooth envelope, and the velocity of the individual wavelets (the phase velocity) is different from the velocity of the envelope (the group velocity). This may be serious evidence for some deep relationship between these phenomena from dissipative and conservative realms. The link in this relationship is cross diffusion, which for NLS is revealed if is rewritten as a system for two real fields u and v via $w = u - iv$ of the form (2) with

$$h_1 = h_2 = 1, \quad D_u = D_v = 0,$$
$$f = u(u^2 + v^2), \quad g = -v(u^2 + v^2).$$

Note the signs of the cross-diffusion terms in the component-wise form of NLS and in (2).

Further investigation has revealed a great variety of the types of nonlinear waves in excitable cross-diffusion systems. In this paper we present some classification of the phenomenologies of such waves.

Our observations are made in two selected two-component kinetic models, supplemented with cross diffusion, rather than self-diffusion terms; such terms may appear, say, in mechanical [8], chemical [2,9], biological, and ecological [10,11] contexts. We note that the case of *only* cross-diffusion terms, with $D_u = D_v = 0$, is special in that the spatial coupling is then not dissipative, and all the dissipation in the system is due to the kinetic terms. So, theoretically speaking, this case may present features that are not characteristic for more realistic models. In practice, however, these worries seem unfounded. Parametric studies done in the past [4,12] indicate that the role of the self-diffusion coefficients D_u, D_v is not essential if they are small enough. Moreover, we have verified that the results presented below are robust in that respect, too. In other words, regimes observed for $D_u = D_v = 0$ typically are qualitatively preserved, even if quantitatively modified, upon adding small D_u, D_v. So in this study we limit consideration to $D_u = D_v = 0$ to reduce number of parameters and focus attention on effects of the cross-diffusion terms. Except where stated otherwise, the values of the cross-diffusion coefficients are $h_1 = h_2 = 1$. We consider the FitzHugh-Nagumo (FHN) kinetics,

$$f = u(u-a)(1-u) - k_1 v, \quad g = \varepsilon u, \tag{5}$$

for varied values of parameters a, k_1, and ε. As a specific example of a real-life system, we also consider the Lengyel-Epstein (LE) [13] model of a chlorite-iodide-malonic acid-starch autocatalitic reaction system

$$f = A - u - \frac{4uv}{1+u^2}, \quad g = B\left(u - \frac{uv}{1+u^2}\right) \tag{6}$$

for varied values of parameters A and B.

II. METHODS

We simulate (2) in one spatial dimension for $x \in [0,L]$, $L \leqslant \infty$, with Neumann boundary conditions for both u and v. We use first-order time stepping, fully explicit in the reaction terms and fully implicit in the cross-diffusion terms, with a second-order central difference approximation for the spatial derivatives. Unless stated otherwise, we used steps $\Delta x = 1/10$ and $\Delta t = 1/5000$ for FHN kinetics (5) and $\Delta x = 0.1$ and $\Delta t = 1/1000$ for LE kinetics (6).

To simulate propagation "on an infinite line," we did the simulations on a finite but sufficiently large L (specified in each case) and instantaneously translated the solution by $\delta x_1 = 30$ away from the boundary each time the pulse, as measured at the level $u = u_*$, where $u_* = 0.1$ for FHN kinetics and $u_* = 1.5$ for LE kinetics, approached the boundary to a distance smaller than $\delta x_2 = 100$, and filled in the new interval of x values by extending the u and v variables at levels $u = u_0$, $v = v_0$, where (u_0, v_0) is the resting state, $u_0 = v_0 = 0$ for FHN kinetics, and $u_0 = A/5$, $v_0 = 1 + A^2/25$ for LE kinetics.

Initial conditions were set as $u(x,0) = u_0 + u_s\,\Theta(\delta - x)$, $v(x,0) = v_0$, to initiate a wave starting from the left end of the domain. Here $\Theta()$ is the Heaviside function, and the wave seed length was typically chosen as $\delta = 2$ or $\delta = 4$. The interval length L was chosen sufficiently large [say, for the system (2,5) it was typically at least $L = 350$] to allow wave propagation unaffected by boundaries, for some significant time.

To characterize shape of the waves emerging in simulations and its evolution, we counted significant peaks (wavelets) in the solutions as the number n of continuous intervals of x where $u - u_0 > 0.1$. In some regimes, this number varied with time, as the shape of enveloped changed while propagating. We also measured the speed of individual wavelets as the speed of the fore ends of these intervals at short time intervals. To estimate the group velocity, we considered the fore edge of the foremost significant peak over a longer time interval, covering several oscillation periods.

To compare the oscillatory front of propagating waves to the linearized theory, we took the v component of the given solution in the interval and selected the connected area in the (x,t) plane where $|v(x,t)| < 0.1$ ahead of the main wave. We numerically fitted this grid function $v(x,t)$ to (7) using Gnuplot implementation of the Marquardt-Levenberg algorithm. The initial guess for parameters C, μ, c, k, x, ω was done "by eye." The fitting was initially on a small interval in time, smaller than the temporal period of the front oscillations, and then gradually extended to a long time interval, so that the result of one fitting was used as the initial guess for the next fitting.

III. RESULTS

A. Overview of wave types

Figure 1 illustrates the three main types of waves in the excitable cross-diffusion system (2) with FHN kinetics (5). Figure 2 explains why these are "main" types. It shows the regions in the parametric plane (a,ε), and we see that the solutions shown in Fig. 1 are represented by large parametric areas. Their common features are quasisoliton interaction and oscillatory front, and the differences are in the propagation mode. A simple quasisoliton [Fig. 1(a), abbreviation SFR in Fig. 2(a)] retains its shape as it propagates. A group, or envelope, quasisoliton [Fig. 1(b), abbreviation SER in Fig. 2(a)] does not have a fixed shape; instead it has the form of spatiotemporal oscillations, whose envelope retains a fixed unimodal shape as it propagates. A multienvelope quasisoliton [Fig. 1(c) and Fig. 1(d), abbreviation MER in Fig. 2(a)] is shown at two time moments, to illustrate the dynamics of its formation. At first, the emerging solution looks like an envelope quasisoliton; however, after some time behind it forms another envelope quasisoliton, then behind that one yet another, and so it continues. The interval of time between formation of new envelopes depends on the parameters; e.g., it becomes smaller for smaller values of a.

Each of the three types of quasisolitons shown in Fig. 1 has a counterpart type of solutions of similar propagation mode, but without the quasisoliton property, i.e., not reflecting upon collision [abbreviations SFN, SEN, MEN in Fig. 2(a)]. Density plots of interaction of the three main types of quasisolitons and their nonsoliton counterparts are shown in Fig. 3. Note that

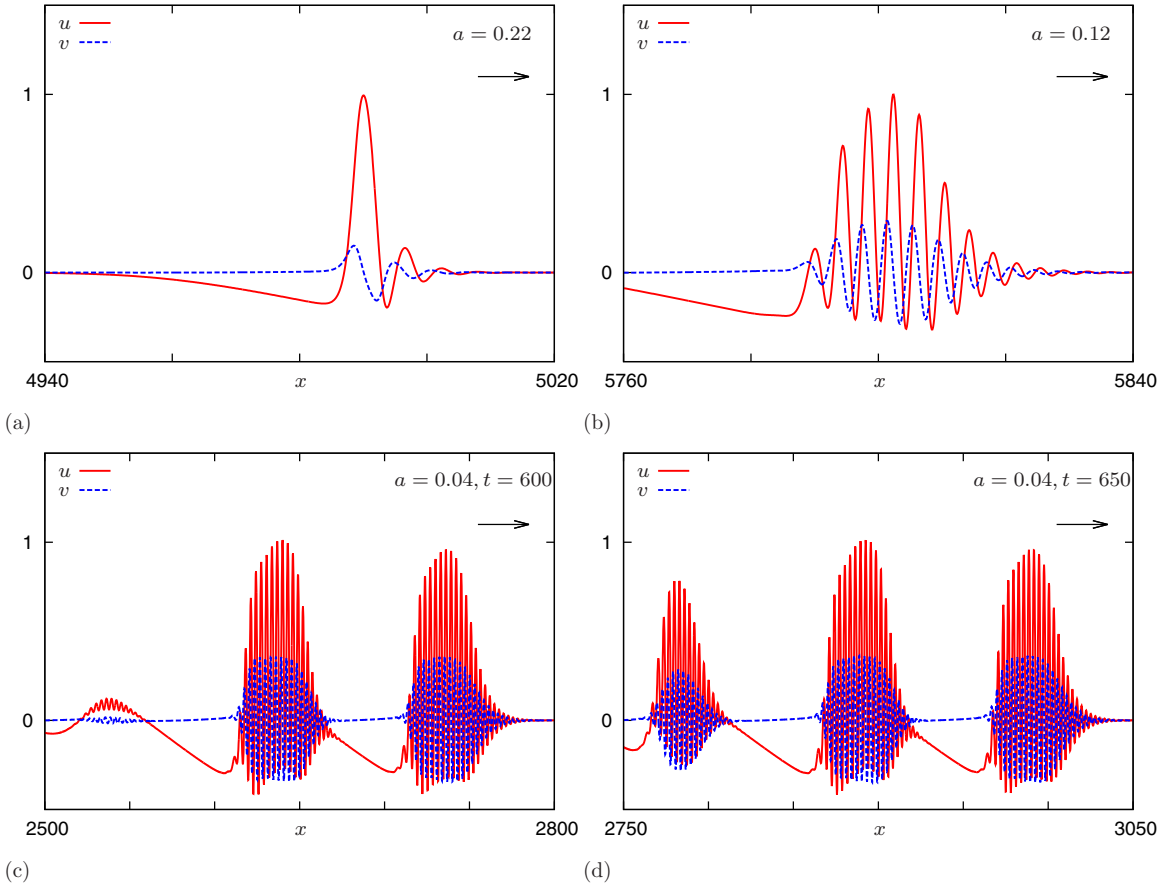

FIG. 1. (Color online) Three typical wave regimes in the cross-diffusion system (2,5) with $k_1 = 10$, $\varepsilon = 0.01$ for different values of a. (a) Simple quasisoliton, $a = 0.22$. (b) Envelope quasisoliton, $a = 0.12$. (c, d) Multienvelope quasiisoliton, $a = 0.04$, at two different time moments.

the nonsoliton regimes do not show immediate annihilation upon the collision. Rather, the process looks like reflection with a decreased amplitude, and subsequent decay; see Fig. 3(d)–3(f).

Apart from the nonreflecting counterparts to the three main types, there are also "nonpropagating" counterparts, all of which are denoted by N in Fig. 2(a). These regimes correspond to waves that are in fact formed from the standard initial

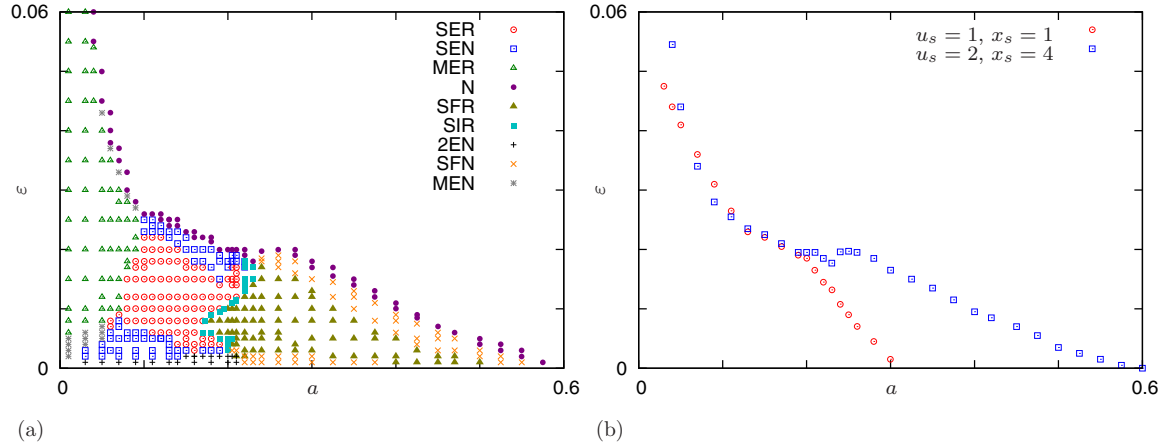

FIG. 2. (Color online) (a) The parametric regions corresponding to different wave regimes in (2,5) in the (a,ε) plane at $k_1 = 10$, $x_s = 4$, $u_s = 2$. The abbreviations in the legend stand for various types of typical wave solutions: SER, single envelope reflecting; SEN, single envelope nonreflecting; MER, multiple envelope reflecting; MEN, multiple envelope nonreflecting; SFR, single fixed-shape reflecting; SFN, single fixed-shape nonreflecting; SIR, single intermediate (between single shape and envelope) reflecting; 2EN, envelope nonreflecting with separate envelopes at the front and at the back with nonoscillating plateau between them; N, no propagation. See Supplemental Material [14] for a movie. (b) Boundaries of the regimes of propagation and decay (of any waves) for different initial conditions.

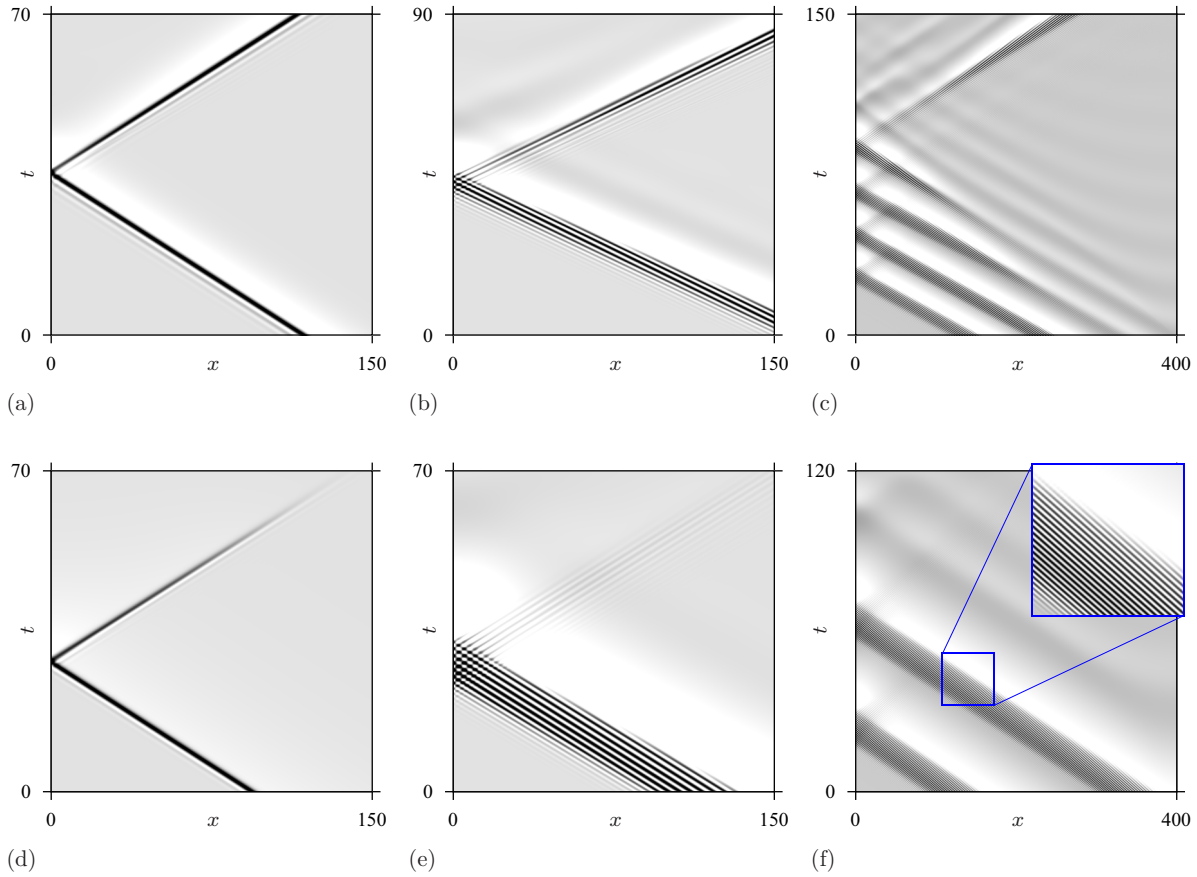

FIG. 3. (Color online) Density plots of impact episodes for selected regimes designated in Fig. 2. (a) SFR: single fixed-shaped ("simple") quasisoliton, $a = 0.22, \varepsilon = 0.01$. (b) SER: single-envelope quasisoliton, $a = 0.1, \varepsilon = 0.01$. (c) MER: multiple envelope quasisoliton, $a = 0.02$, $\varepsilon = 0.01$. In the panel, only the first reflected envelope has almost recovered within the view; other envelopes recover later. (d) SFN: single fixed-shape nonreflecting wave, $a = 0.45$, $\varepsilon = 0.004$. (e) SEN: single-envelope nonreflecting wave, $a = 0.1$, $\varepsilon = 0.004$. (f) MEN: multiple envelope nonreflecting wave, $a = 0.02$, $\varepsilon = 0.004$. In (c) and (f), individual wavelets are not distinguishable at printing resolution so only the envelope is in fact seen; in (f) the fine structure of the wavelets is shown magnified in the inset. White corresponds to $u = -0.3$, black corresponds to $u = 1$. Time reference point $t = 0$ is chosen arbitrarily at the beginning of the selected episode; point $x = 0$ corresponds to the left boundary of the interval. All simulations are done for $\Delta x = 0.1$, $\Delta t = 0.001$, $L = 400$, $k_1 = 10$.

conditions, but then decay after some time. Naturally, the success of initiation of a propagating wave does in fact depend on the parameters of the initial conditions: Fig. 2(b) shows how the region of single quasisoliton differs for two different initial conditions. This is of course expectable for excitable kinetics.

The analysis of the dynamics of the wavelets and wave speeds for the three main types of quasisolitons, illustrated in Figs. 4 and 5, reveals the following:

(1) The amplitude and speed of the simple quasisolitons do not change in time [Fig. 4(a) and 4(d)].

(2) For the envelope and multienvelope quasisolitons, the amplitudes of individual wavelets during their lifetime first grow to a certain maximum and then decrease monotonically [Fig. 4(b) and 4(c)]. The speed of a wavelet (the phase velocity) is high at first, but then decreases nonmonotonically [Fig. 4(e) and 4(f)].

(3) In the process of establishment of an envelope quasisoliton, the number of wavelets in it increases until saturation [Fig. 5(a)], and so does the speed of the envelope (the group velocity) [Fig. 5(e)].

(4) Figure 5(b) and 5(f) shows that in simple quasisolitons ($a > 0.2$), the number of wavelets remains the same ($n = 2$), and their speed remains approximately the same in that interval; whereas in envelope quasisolitons ($a < 0.2$), both the number of wavelets and their velocities increase with the decrease of a.

(5) Figure 5(c) and 5(g) shows that increase of parameter ε causes decrease of both the number of wavelets and of their speeds.

(6) Parameter k_1 also plays a significant role in defininig the wave regime and its parameters [Fig. 5(d) and 5(h)].

The oscillatory character of the fronts of cross-diffusion waves both for simple quasisolitons and for envelope quasisolitons, which is apparent from numerical simulations, is easily confirmed by linearization of (2) around the resting state. The resting states in both FHN (5) and LE (6) kinetics are stable foci which already show propensity to oscillations. Taking the solution of the linearized equation in the form

$$\begin{bmatrix} u - u_0 \\ v - v_0 \end{bmatrix} \approx \mathrm{Re}(C\mathbf{v}e^{-\mu(x-ct)}e^{i(kx-\omega t)}), \tag{7}$$

we need

$$\mathbf{A}(\lambda,\nu)\mathbf{v} = \mathbf{0}, \quad \mathbf{v} \neq \mathbf{0}, \quad \det \mathbf{A} = 0, \tag{8}$$

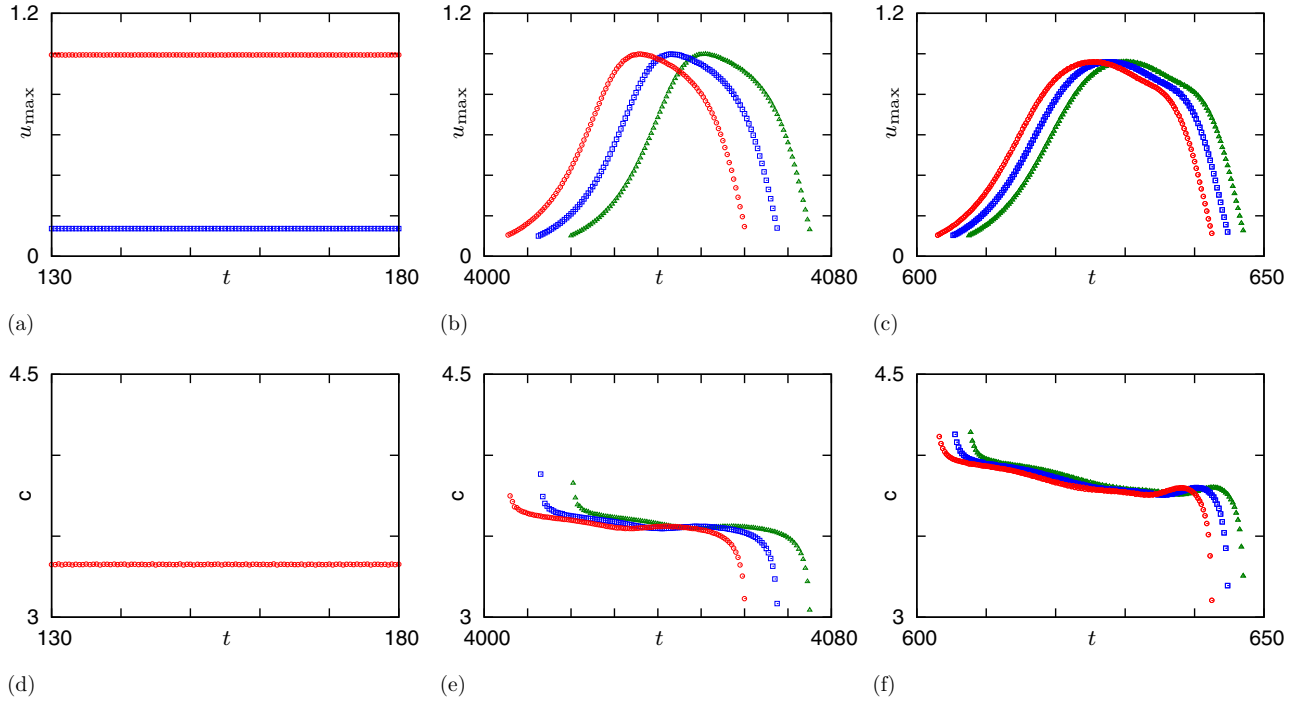

FIG. 4. (Color online) Dynamics of (a–c) amplitudes and (d–f) velocities of individual wavelets for the three types of quasisolitons in (2,5) for $k_1 = 10$, $\varepsilon = 0.01$. (a, d) Simple quasisoliton, $a = 0.22$; see Fig. 1(a). (b, e) Envelope quasisoliton, $a = 0.12$; see Fig. 1(b). (c, f) Multienvelope quasisolitons, $a = 0.04$; see Fig. 1(c, d).

where

$$\mathbf{A} = \begin{bmatrix} -a-\lambda & -k_1+\nu^2 \\ \varepsilon-\nu^2 & -\lambda \end{bmatrix},$$
$$\lambda = \mu c - i\omega,\ \nu = -\mu + ik.$$

Equation (8) imposes two constraints (for the real and imaginary parts of the determinant) on the four real quantities μ, c, k, and ω, so it is by far insufficient to determine the selection of these parameters, but this equality can be verified for the numerical simulations, in order to ensure that the

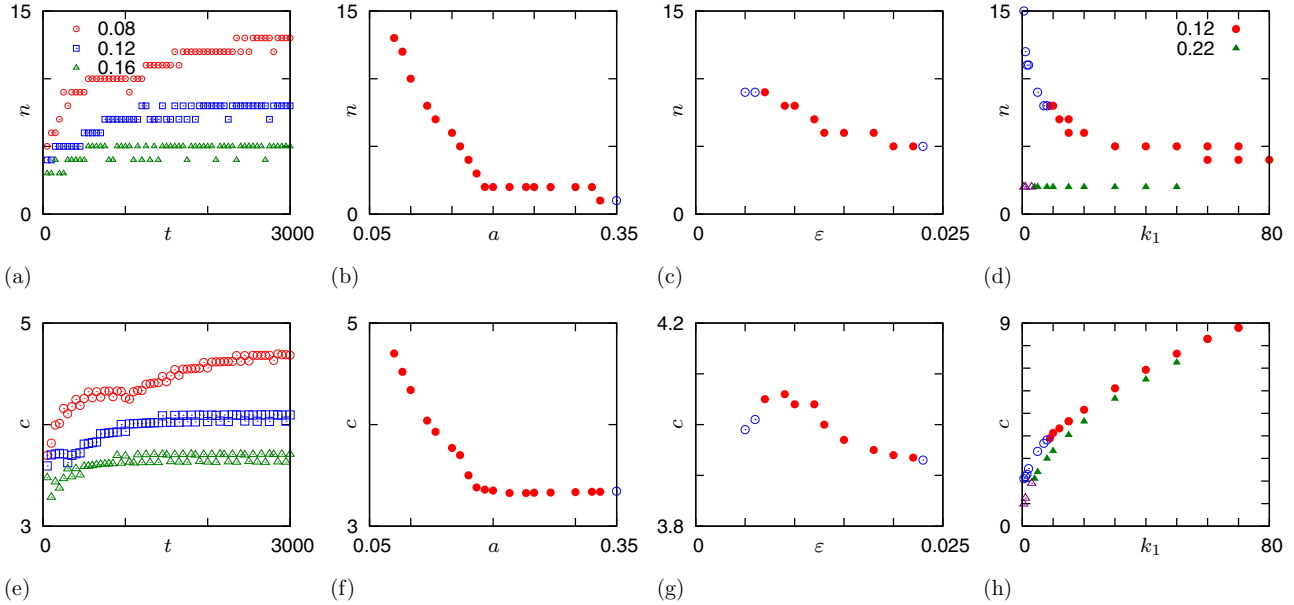

FIG. 5. (Color online) (a–d) Number of wavelets and (e–h) velocities of the envelope waves in transient and in established regimes. (a, e) The transients for $k_1 = 10$, $\varepsilon = 0.01$ and three values $a = 0.08$ (circles), 0.12 (squares) and 0.16 (triangles). (b, f) Established quantities as functions of parameter a for fixed $k_1 = 10$, $\varepsilon = 0.01$. (c, g) Established quantities as functions ε for fixed $a = 0.12$, $k_1 = 10$. (d, h) Established quantities as functions k_1 for fixed $\varepsilon = 0.01$ and $a = 0.12$ (circles) and $a = 0.22$ (triangles). In (b–d) and (f–h), filled symbols designate quasisoliton (reflecting) waves, and open symbols designate nonreflecting waves.

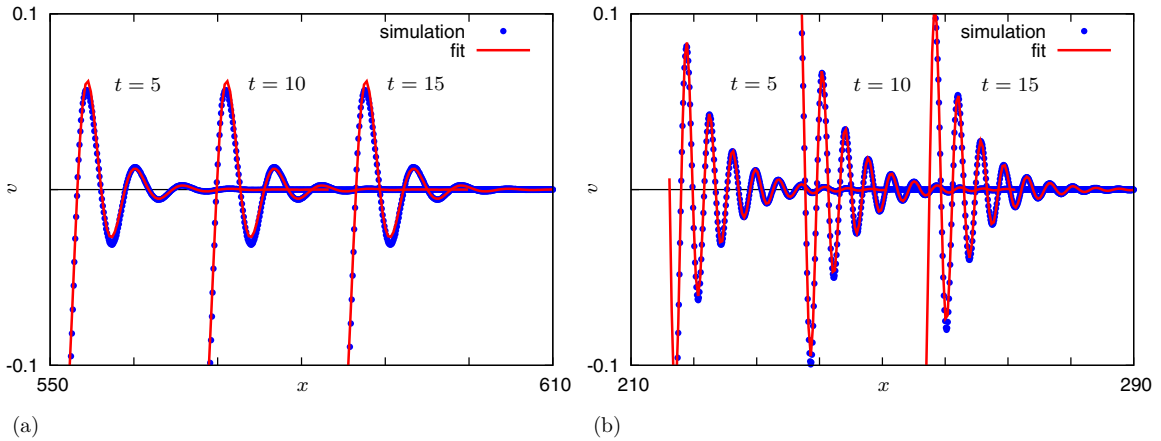

FIG. 6. (Color online) Profiles of established propagating waves at selected moments of time for $k_1 = 10$, $\varepsilon = 0.01$, $L = \infty$. The origins of the t and x axes are chosen arbitrarily. (a) Simple quasisoliton, $a = 0.22$. (b) Envelope quasisoliton, $a = 0.12$.

observed oscillatory fronts are not a numerical artifact but a true property of the underlying partial differential equations. Hence we fitted selected simulations around the fronts with the dependence (7). The quality of the fitting is illustrated by two examples in Fig. 6. The fitted parameters satisfied (8) with good accuracy; in both cases, they gave $|\det \mathbf{A}/(\mathrm{Tr}\,\mathbf{A})^2| < 10^{-3}$.

Note that the approximation (7) makes explicit the concepts of wavelets (the oscillating factor $e^{i(kx-\omega t)}$), the phase velocity (the ratio ω/k), the envelope (in this case the exponential shape $e^{-\mu(x-ct)}$), and the group velocity (the fitting parameter c). As expected, for the simple quasisoliton shown in Fig. 6(a) the fitted group and phase velocities coincided within the precision of fitting ($|c - \omega/k| < 10^{-5}$). For the envelope quasisoliton shown in Fig. 6(b) they were significantly different: $c \approx 4.077$, $\omega/k \approx 3.586$.

B. Multienvelope quasisolitons

We use the term multiplying envelope quasisolitons (MEQS) to concisely designate spontaneously multiplying envelope quasisolitons. The process of self-multiplication leads to eventually filling the whole domain, behind the leading edge of the first group, with what appears as a train of envelope quasisolitons, i.e., a hierarchical, quasiperiodic regime. This is illustrated in Fig. 7(a) for periodic boundary conditions, the setting that eliminates the "leading edge" complication mentioned above. One envelope quasisoliton (EQS) produced by the standard initial conditions develops an instability at its tail, leading to generation of the second EQS ($t = 230$). The system of two EQSs generates a third ($t = 420$). After forming of a system of five EQSs ($t = 600$), the inverse transition happens, from five to four envelopes ($t = 1430$, $t = 1630$), and then from four to three envelopes ($t = 1980$, $t = 2270$), leading to an established, persistent state of three envelopes ($t = 4050$). The same process is represented also as a density plot in Fig. 7(b).

Panels (a) and (d) of Fig. 8 analyze the dynamics of the number of wavelets and the group (envelope) velocity for the simulation shown in Fig. 7. Both the wavelet number and the group velocity grow, albeit nonmonotonincally, till reaching stable constant values, which corresponds to establishment of the stationary regime of three envelopes shown in Fig. 7. We stress that the group velocity of the established multienvelope soliton regime in a circle is always higher than the speed of a similar regime on the "infinite line," which is illustrated in Fig. 8(b) and 8(e): there the speed is established monotonically, and the number of envelopes constantly increases. In Ref. [15] we have demonstrated that in a cross-diffusion excitable system, the speed of a periodic train of waves can be faster for smaller periods. There we called this effect "negative refractoriness," meaning, using electrophysiological terminology, that in the relative refractory phase the excitability is enhanced rather than suppressed. In the present case, we observe a similar negative refractoriness effect on the higher level of the hierarchy, for envelope quasisolitons (groups of waves) rather than individual waves.

To conclude the analysis of the wavelet number and group speeds for multienvelope quasisolitons, we note that for the MEQS on an "infinite line," as should be expected, does not depend on the length of the interval used for computations, and the number of envelope, obviously, does; see Fig. 8(c) and 8(f).

C. Lengyell-Epstein kinetics

Results of our numerical experiments with the reaction–cross-diffusion system (2) with the LE kinetics (6) are qualitatively similar to those with the FHN kinetics (5), described above. Figure 9 illustrates the collision of an EQS with an impremeable boundary for the LE kinetics. We can see that the amplitudes of the wavelets decrease upon the collision ($t = 330$) and then recover to their stationary values ($t = 580$, $t = 610$). Similarly, Fig. 10 illustrates formation of MEQS and their interaction with the boundary for the LE kinetics. The parametric portrait in the (A, B) plane is shown in Fig. 11. All the qualitatively distinct regimes identified for the FHN kinetics and shown in Fig. 2, have been also found for the LE kinetics and shown in Fig. 11.

D. More exotic regimes

Finally, we consider two more regimes to complete our overview.

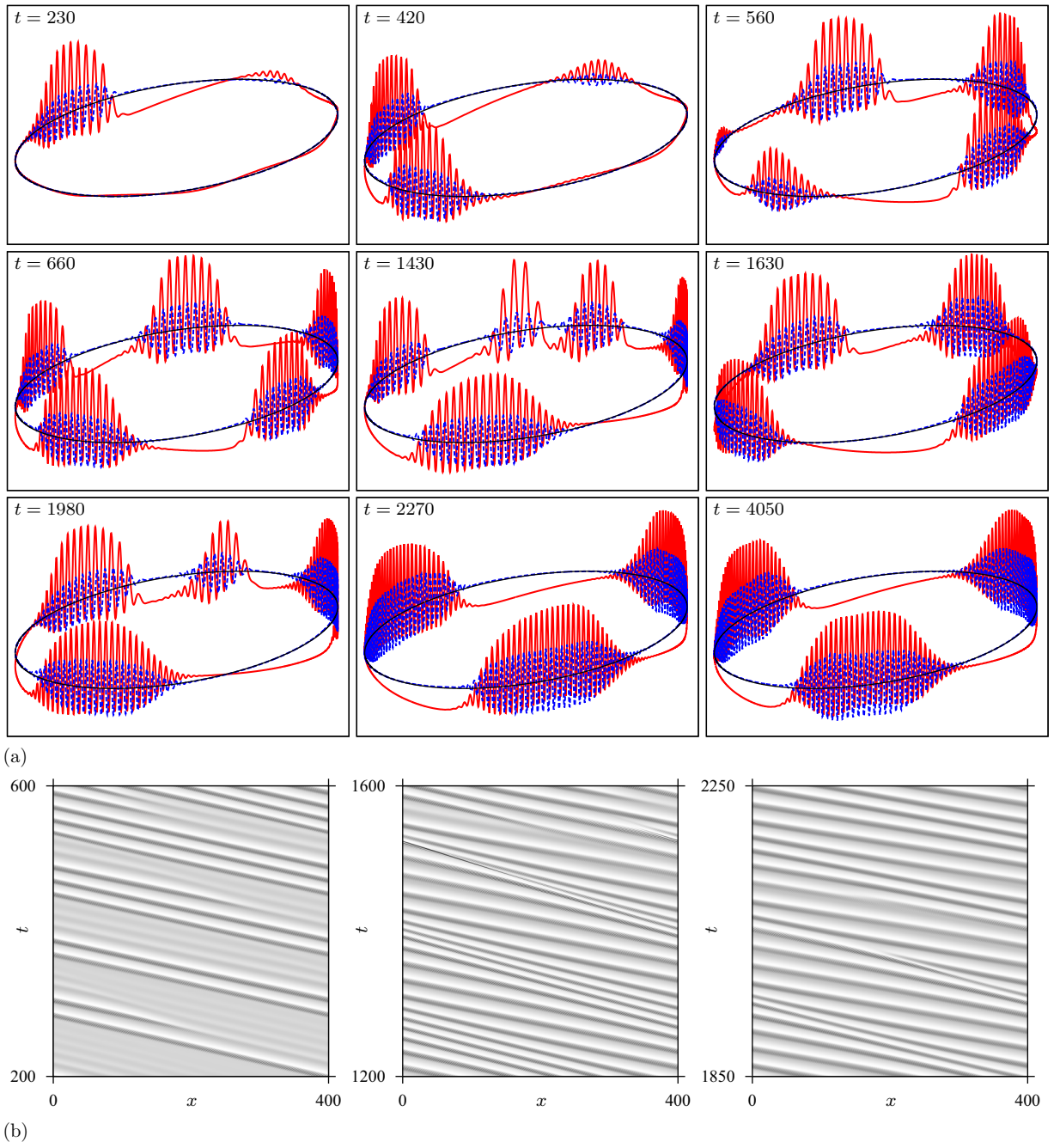

FIG. 7. (Color online) Formation and evolution of a multienvelope quasisoliton regime on a circle (one-dimensional cable with periodic boundary conditions), for $a = 0.03$, $k_1 = 10$, $\varepsilon = 0.01$. (a) Snapshots of the profiles at selected moments of time. The waves and wavelets propagate counterclockwise. (b) Density plots of the u component of the solution for selected time intervals; white corresponds to $u_{\min} = -0.2$, black corresponds to $u_{\max} = 1$ corresponds to black. See also the movie in the Supplemental Material [14].

The "single intermediate reflecting" (SIR) regime found both in Fig. 2(a) and Fig. 11 is "intermediate" in the sense that it periodically changes its shape as it propagates, in which sense it is similar to the envelope quasisoliton; however, most of the time it propagates nearly as a simple quasisoliton. Only during relatively short episodes, the wave undergoes transformation, whereby it looses a wavelet at the tail and begets one at the front, and these episodes are separated by relatively long periods when the wave retains a constant shape. The dynamics of the parameters of such a regime is shown in Fig. 12(a), (b), (d), and (e). This phenomenology is reminiscent of a limit cycle born through bifurcation of a homoclinic orbit. In our present context, this would of course be an equivariant bifurcation with respect to the translations along the x axis, or the bifurcation in the quotient system, i.e., the system describing the evolution of the shape of the propagating wave, as opposed to position of that wave (see Refs. [16–19]). Correspondingly, the limit cycle presents itself as the periodic repetition of the shapes of the

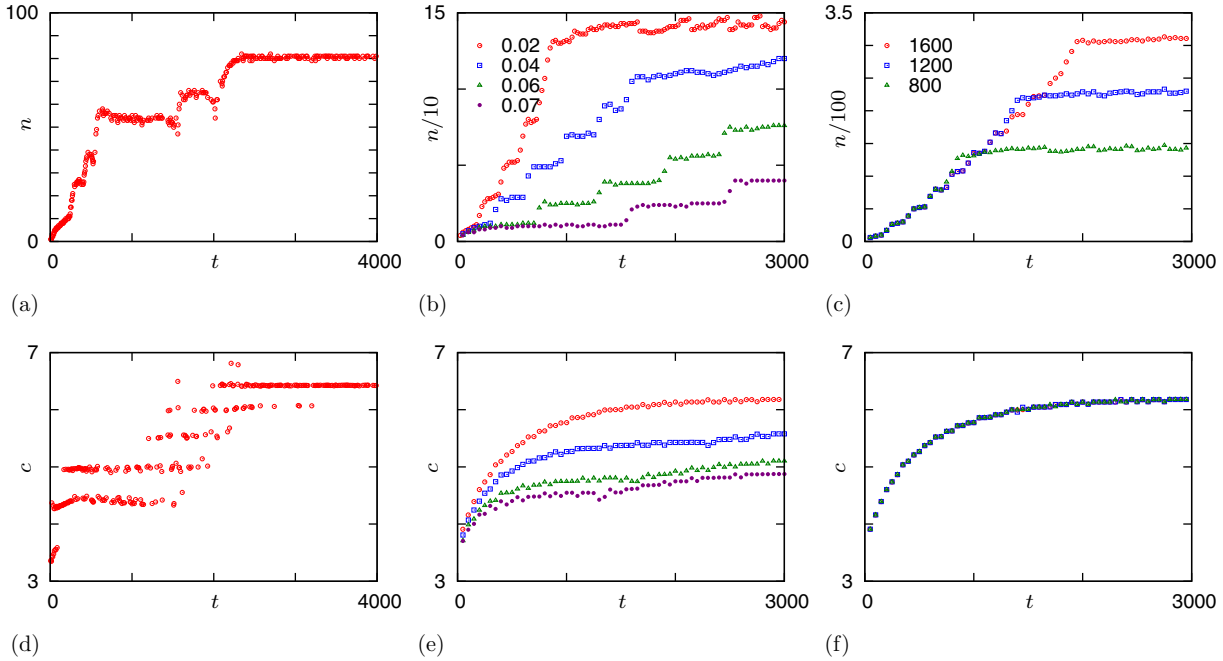

FIG. 8. (Color online) The dynamics of (a–c) numbers of wavelets and (e–h) velocities of the envelope waves in multienvelope quasisoliton regimes. (a, d) The quantities measured in a finite L with periodic boundary conditions; the same simulation as shown in Fig. 7. (b, e) The quantities are measured for the headmost $L = 800$ interval of a wave train in an "infinite length" computations, for $\varepsilon = 0.01$, $k_1 = 10$ and selected values of a as indicated in the legend. (c, f) The quantities are measured for $\varepsilon = 0.01$, $k_1 = 10$, and $a = 0.02$, with different measurement length L as indicated in the legend. In panel (f), the velocities measured for different L are indistinguishable.

quasisolitons, rather than periodic solutions in the usual sense. In the qualitative theory of ordinary differential equations, there are two classical examples, which predict different dependencies of the period on the bifurcation parameter. One is the bifurcation of a homoclinic loop of a saddle point [20]; the other is the bifurcation of a homoclinic loop of a saddle node [21], also known as SNIC (saddle node in the invariant circle) bifurcation, SNIPER (Saddle-Node Infinite Period) bifurcation, and "infinite period" bifurcation; see, e.g., Ref. [22, chap. 8.4]. In the case of a homoclinic of a saddle, the expected dependency is

$$T \approx C_1 + C_2 \ln(|a - a_*|), \tag{9}$$

where a_* is the critical value of the bifurcation parameter a and C_1 and C_2 are some constants. For the bifurcation of the

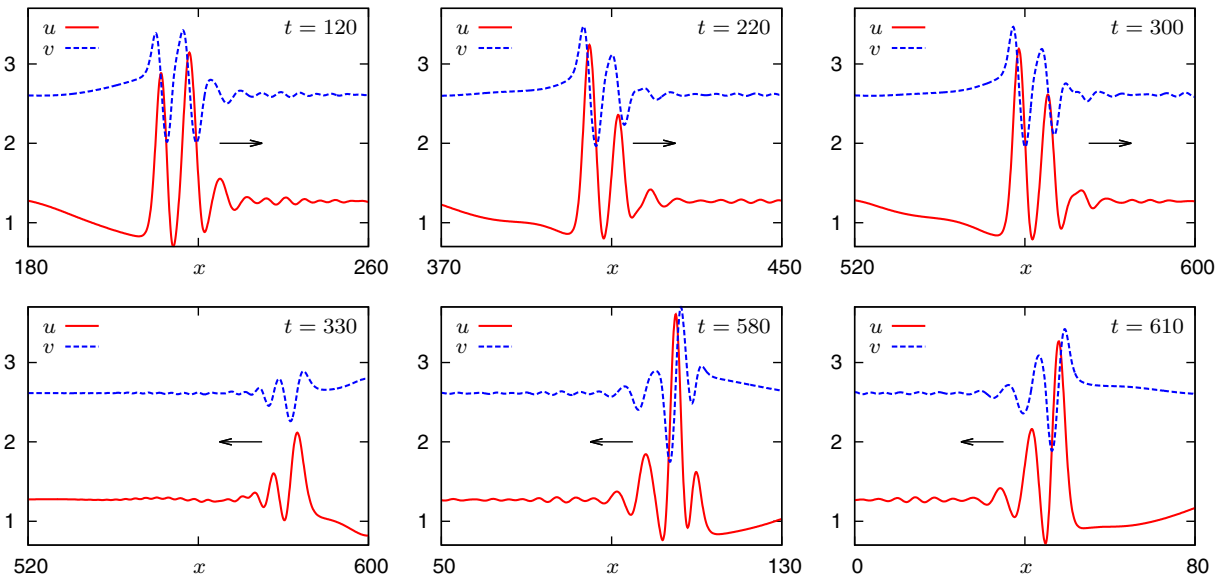

FIG. 9. (Color online) Quasisoliton interaction of an envelope soliton with an impermeable boundary in LE model (2,6), $A = 6.35$, $B = 0.045$.

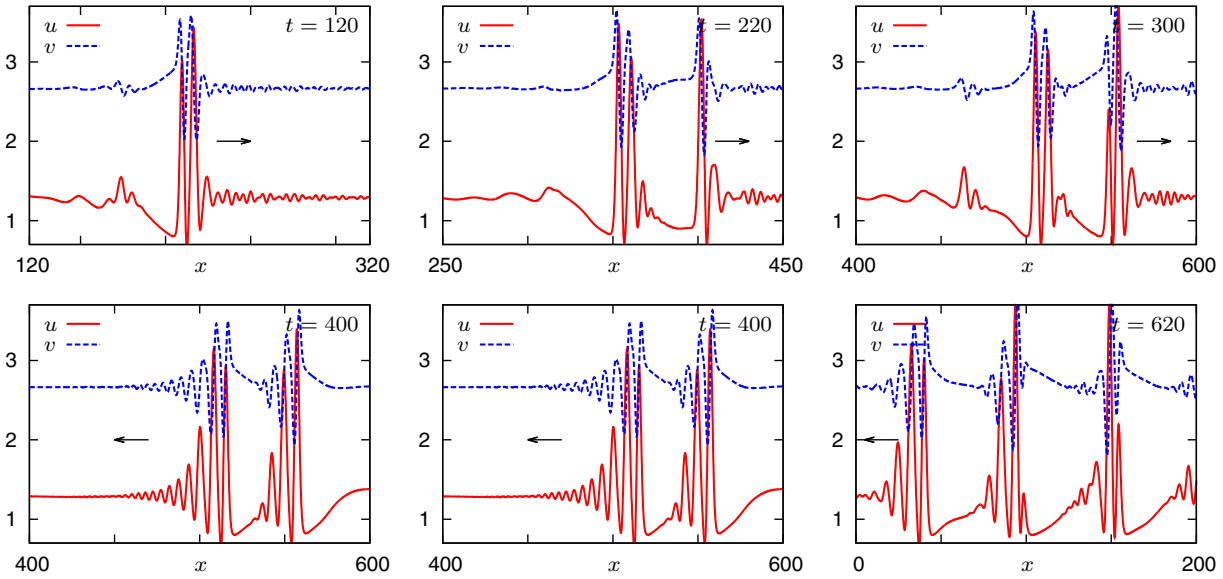

FIG. 10. (Color online) Formation of a multienvelope quasisoliton and its interaction with an impermeable boundary in LE model (2,6), with $A = 6.45$, $B = 0.045$.

homoclinic loop of a saddle node, the asymptotic is different,

$$T \approx C_3|a - a_*|^{-1/2} \tag{10}$$

for some constant C_3. The fitting of the dependence of the soliton shape period on the bifurcation parameter a in the FHN kinetics by (9) and (10) is shown in Fig. 12, panels (c) and (f), respectively. In our case, the hypothetical limit cycles exist for $a < a_*$, and the best-fit bifurcation value for (9) is $a_* \approx 0.206477$, whereas for (10) it is $a_* \approx 0.206925$.

The other regime is "double-envelope nonreflecting" (2EN), and it has separate "envelope" trains at the front and at the back, separated by a nonoscillating plateau; see Fig. 13. The corresponding dynamics of the wavelet amplitudes and their speeds is shown in Fig. 14. This regime is observed for smaller values of ε in the FHN kinetics [Fig. 2(a)] and smaller values of B in the LE kinetics (Fig. 11).

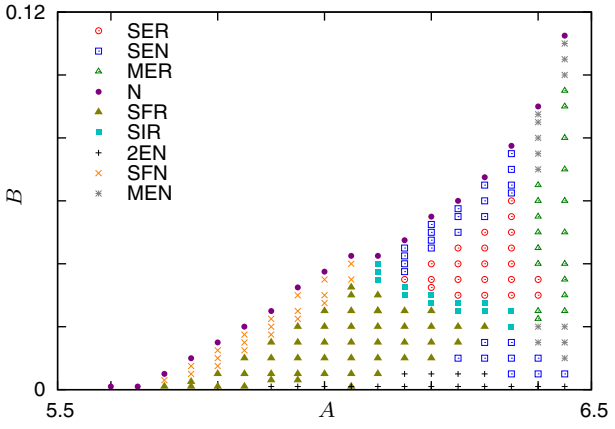

FIG. 11. (Color online) Parametric regions in the (A, B) plane for different wave regimes in LE model (2,6),. The nomenclature of the wave regimes is the same as in Fig. 2.

E. Quasisolitons in two spatial dimensions

In Ref. [23] we have shown that simple quasisoliton waves in two-dimensional excitable systems with cross diffusion can penetrate or break on collision. Whether the wave break occurs or not depended on curvature and thickness of the waves, and also on the angle of their collision, leading to emergence of complicated patterns. The two-dimensional extensions of the envelope and multienvelope quasisolitons are no simpler, and we present here only a few selected examples; see Figs. 15–17. The wave breaks can occur to whole wave trains, as well as modify the number of a wavelets in a train, and the result of a collision depends on the time interval since a previous collision, so that encounters occurring in a quick succession are more likely to lead to wave breaks. This can lead to "wave flocks," that is, wave groups bounded not only lenthwise but also sidewise; see Figs. 15 and 17. For comparison, Fig. 16 shows development of a "wave grid" of two-dimensional simple quasisolitons, i.e., the case where every wave has exactly one wavelet; another reason for a different appearance is that the waves at these parameters are more robust than those in Figs. 15 and 17, and are broken less often, hence the typical sidewise extent of the wave fragments is significantly longer.

IV. DISCUSSION

Solitons have attracted an enormous attention both from mathematical viewpoint and from applications ever since their discovery. For applications, it has been always understood that the classical solitons are an idealization, and it is therefore interesting to study systems and solutions similar to solitons in different aspects and in various degrees. Zakharov and Kuznetsov [24], discussing optical solitons, commented (translation is ours): "Objects called solitons in nonlinear optics are not solitons in the strict sense of the word. Those are quasisolitons, approximate solutions of the Maxwell equations, depending on four parameters. Real stationary

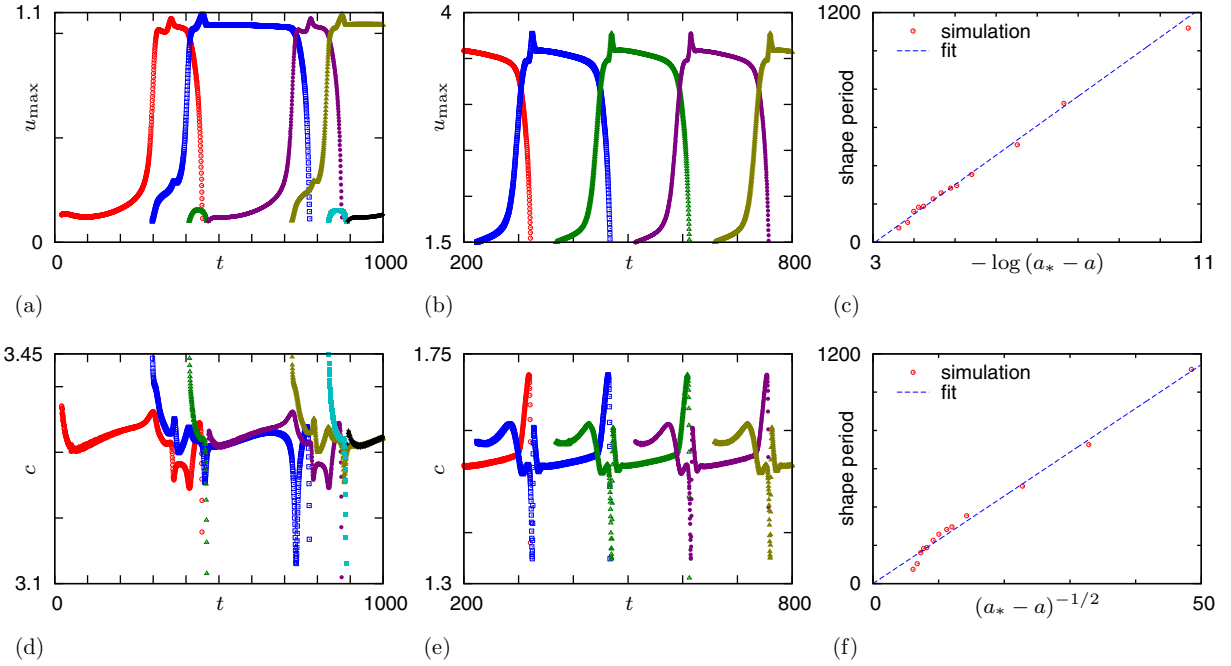

FIG. 12. (Color online) Dynamics of quasisolitons in the transitional area "SIR" in Figs. 2(a) and 11. (a, b) amplitudes and (d, e) velocities of individual wavelets of quasisolitons. (a, d) FHN model (2,5), $a = 0.18$, $\varepsilon = 0.006$. (b, e) LE model (2,6), $A = 6.25$, $B = 0.025$. (c, f) Dependence of the quasisoliton shape change period in the FHN model as a function of parameter a at fixed $\varepsilon = 0.005$, and its best fits by the theoretical dependencies (9) and (10), respectively. See the last episode of the Fig02 movie in the Supplemental Material [14].

solitons, which propagate with constant speed and without changing their form, are exact solutions of the Maxwell equations, depending on two parameters." We mention in passing that we are using the word "quasisolitons" in a different sense than in Ref. [24]; however, the main message is that the completely integrable systems like nonlinear Schrödinger equation are always an idealization, and in real life one is interested in broader class of equations and a broader class of solutions.

The nonlinear dissipative waves in excitable and self-oscillatory systems are traditionally considered an entirely different sort of things from the integrable systems displaying the classical solitons: the words "active media" and "autowaves" are sometimes also used to characterize this different "world."

The excitable media with cross diffusion that we considered in this paper are somewhat intermediate in that they present features in common to both these different "worlds." On one hand, in a large areas of parameters, we observe reflection from boundaries and penetration through each other, although with a brief decrease, but without change in shape and amplitude in the long run. The link to dissipative waves is that in the established regimes have amplitude and speed depending on the system parameters rather than initial conditions.

In this paper, we have reviewed parametric regions and properties of a few different regimes, such as simple quasisolitons (corresponding to classical solitons in integrable systems) and envelope quasisolitons (corresponding to envelope, or group solitons, or breathers in integrable systems). We have identified a transitional region between simple and envelope quasisolitons, which displays features of a homoclinic bifurcation in the quotient system. We also have described a regime we called multienvelope quasisolitons. This regime presents a next level of hierarchy, after simple quasisolitons ("solitary" wave, stationary solution in a comoving frame of reference) and envelope quasisolitons ("group" wave, periodic solution in a comoving frame of reference), which are "groups of groups of waves" and apparently quasiperiodic solutions in a comoving frame of reference. One naturally wonders if this is the last level in this hierarchy or more complicated structures may be observed after a more careful consideration; however, this is far beyond the framework of the present study.

We have limited our consideration, with two simple exceptions, to a purely empirical study, leaving a proper theoretical investigation for the future. The two exceptions are that we confirm that the oscillating fronts of the simple quasisolitons and envelope quasisolitons observed in numerical simulations are in agreement with the linearized theory, and that the periods of the quasisolitons in the transitional zone between simple and envelope are consistent with a homoclinic bifurcation in a comoving frame of reference. Further theoretical progress may be achievable either by studying of the quasisoliton solutions as boundary-value problems by their numerical continuation and bifurcation analysis, or by asymptotic methods. At present we can only speculate that one possibility is the limit of many wavelets per envelope, which is inspired by observation that in this limit the shape of the wavelets is nearly sinusoidal, so some kind of averaging procedure may be appropriate in which the fast-time "wavelet" subsystem is linear and the nonlinearity only acting in the averaged slow-time "envelope" subsystem. We have already commented in Ref. [6] that treating cross-diffusion FitzHugh-Nagumo system as a dissipative perturbation of the nonlinear Schrödinger equation does not work out. A further observation is that apparently this separation of time scales cannot be uniform, as some parts

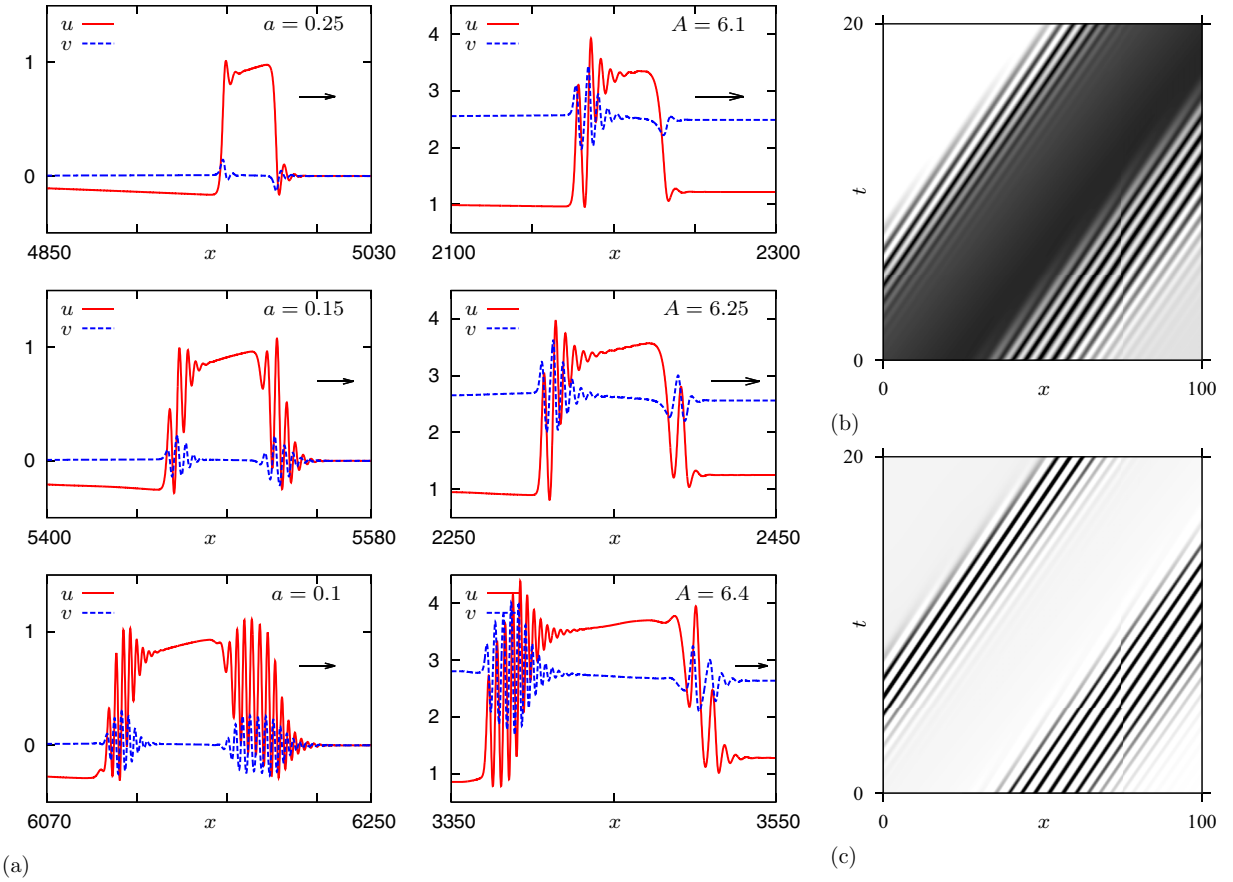

FIG. 13. (Color online) (a) Profiles of established wave regimes for parameters from the "Z" zones in Figs. 2(a) and 11. Left column: FHN model (2,5) for $\varepsilon = 0.001$ and $a = 0.25$, $a = 0.15$ and $a = 0.1$ as shown by the legends. Right column: LE model (2,6) for $B = 0.001$ and $A = 6.1$, $A = 6.25$ and $A = 6.4$, as shown by the legends. (b, c) Fragment of a density plot of, respectively, the u and v variables for the FHN model with $a = 0.1$.

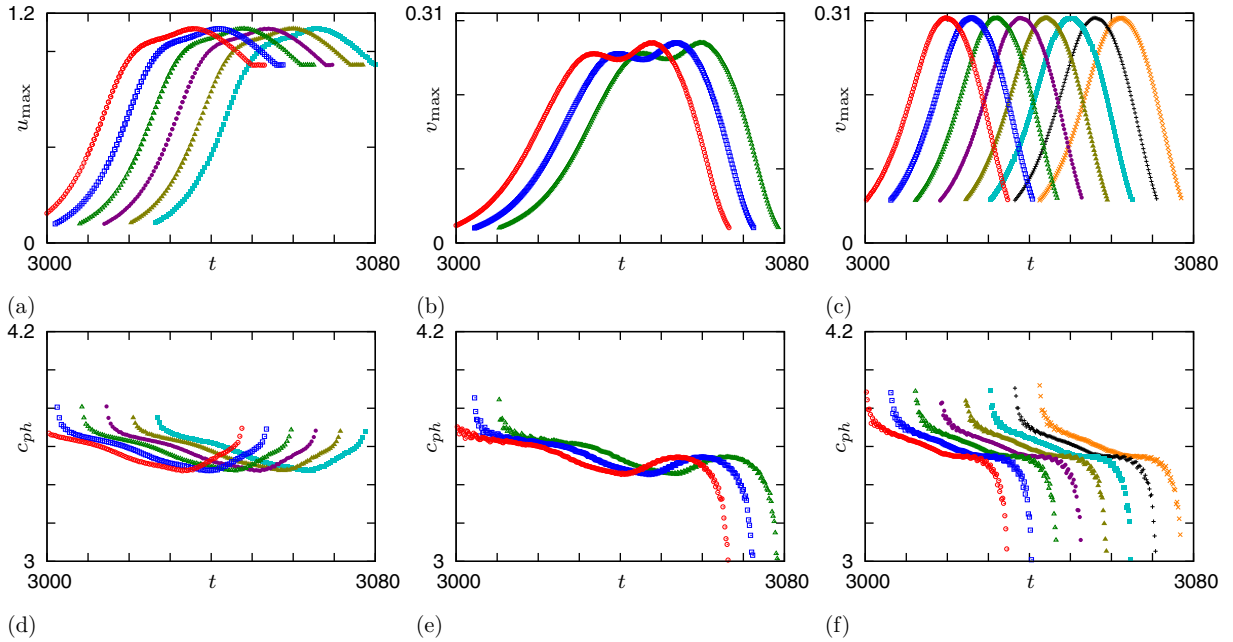

FIG. 14. (Color online) Dynamics of the (a–c) amplitudes and (d–f) velocities of individual wavelets, (a, d) of the u variable in the front zone, (b, e) of the v variable in the front zone, (c, f) of the v variable in the back zone, for the FHN model (2,5) at $k_1 = 10$, $a = 0.1$, $\varepsilon = 0.001$; see top bottom left panel of Fig. 13(a).

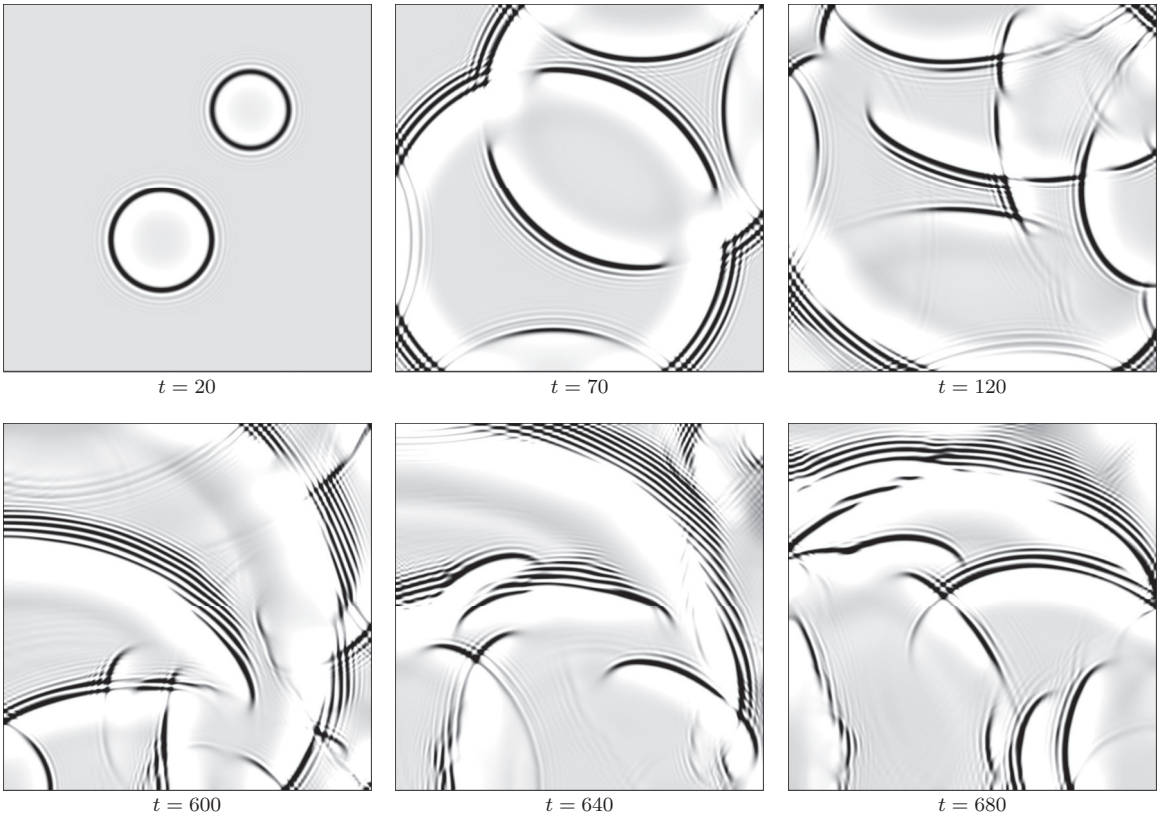

FIG. 15. Selected snapshots of "wave flocks" of envelope quasisolitons in 2D FHN model with $a = 0.02$, $\varepsilon = 0.01$, $k_1 = 5$, $h_1 = h_2 = 0.3$, box size 140×140. See Supplemental Material [14] for a movie.

of the envelope quasisolitons that indeed look as amplitude-modulated harmonic "AC" oscillations with a slow "DC" component, such as the head and the main body of the EQS illustrated in Fig. 1(b), and the "front" and "back" oscillatory pieces of the "double-envelope" regime shown in Fig. 13, and some other parts which have only the slow component but no oscillating component, such as the tail of the EQS of Fig. 1(b) and the plateau and the tail of the double-envelope wave of Fig. 13. This suggests that any asymptotic description of these waves will have to deal with matched asymptotics.

The systems we consider are not conservative, and the natural question is where such systems can be found in nature. We have mentioned in the Introduction a number of applications that motivate consideration reaction-diffusion system with cross-diffusion components; a more extensive discussion of that can also be found in Ref. [2]. Regimes resembling quasisolitons and finite-length wave trains phenomenologically have been observed in various places. The review [2] describes a number of unusual wave regimes obtained in BZ-type reactions in microemulsions, including, e.g., "jumping waves" and "packet waves," which share some

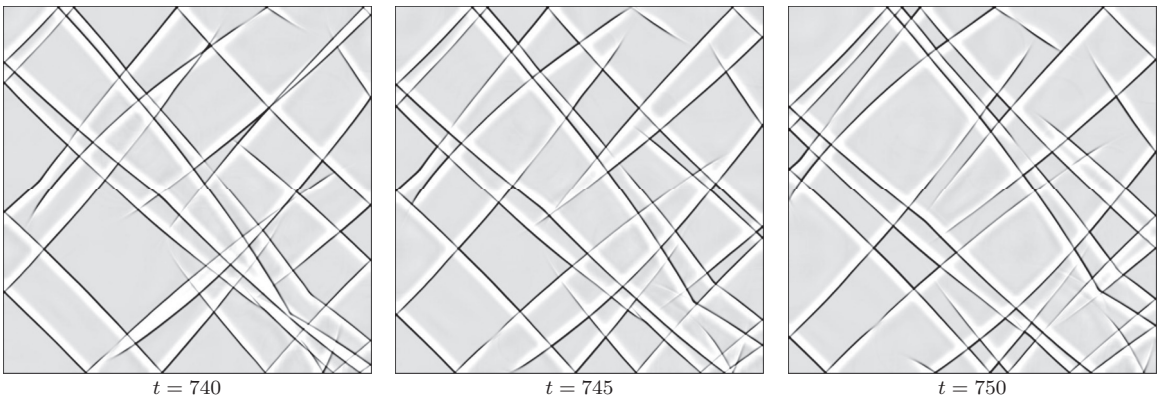

FIG. 16. Selected snapshots of "wave grid" of quasisolitons in 2D FHN model with $a = 0.02$, $k_1 = 30$, $\varepsilon = 0.01$, $h_1 = h_2 = 0.1$, box size 140×140. See Supplemental Material [14] for a movie.

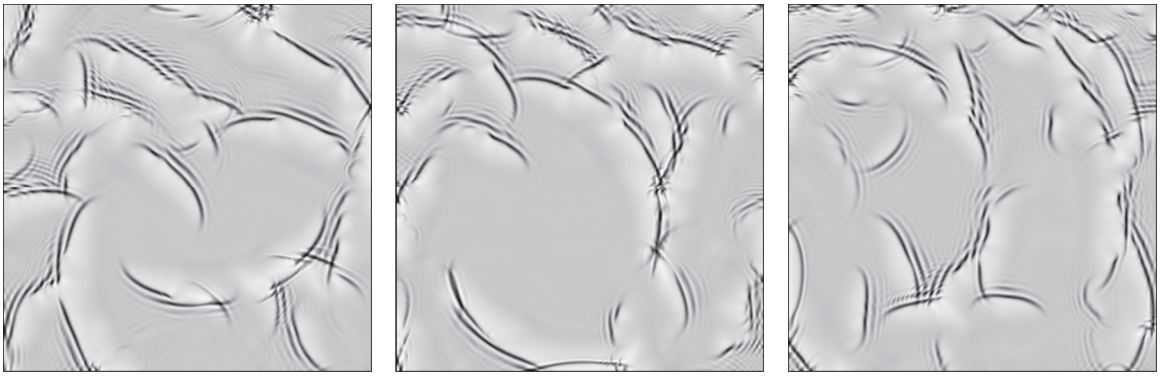

FIG. 17. Selected snapshots of "wave flocks" of envelope quasisolitons in 2D LE model with $A = 6.4$, $B = 0.04$, $h_1 = 0.3$, $h_2 = 0.3$, box size 140×140. See Supplemental Material [14] for a movie.

phenomenology with the group quasisolitons. The "packet waves" are considered in more detail in Refs. [25,26], which demonstrate, in particular, cases of quasisolitonic behavior of those, i.e., reflection from boundaries, see Fig. 5(e) in Ref. [26], although it is difficult to be sure if it is the same as our group quasisolitons as too little detail are given. Those packet waves have been reproduced in a model with self-diffusion only, but with three components. Another example of complicated wave patterns which may be related to quasisolitons is given in Ref. [27], with experimental observations in a variant of BZ reaction as well as numerical simulation; again the simulations there were for a three-component reaction-diffusion system with self-diffusion only. Regarding chemical systems, we must note that the models we considered here may not be expected to be realized literally. Apart from the choice of the kinetic functions and particularly of their parameters, based more on mathematical curiosity than real chemistry, the linear cross-diffusion terms as in (2) cannot describe real chemical systems as they do not guarantee positivity of solutions for positive initial conditions, so system (2) can only be considered as an idealization of (3), with corresponding restrictions. Further, our choice of the diffusivity matrix appears to be in contradiction with physical constraints related to the Second Law of Thermodynamics, which in particular require that the eigenvalues of the diffusivity matrix are real and positive, whereas ours are complex; see, e.g., Ref. [2, p. 899] for a discussion. From this viewpoint, with respect to chemical systems, our solutions may be only considered as "limit cases," presenting regimes which possibly may be continued to parameter values that are physically realizable. On the other hand, it is well known that the aforementioned constraints apply to the *actual* diffusion coefficients, whereas mathematical models obtained by asymptotic reduction deal with *effective* diffusion coefficients, and the effective diffusion matrices may well have complex eigenvalues. A famous example is the complex Ginzburg-Landau equation (CGLE); see, e.g., Ref. [28, Appendix B]. This equation for one complex field, sometimes called an "order parameter," emerges as a normal form of a supercritical Hopf bifurcation in the kinetic term of a generic reaction-diffusion system. This equation can also be written, in turn, as a two-component reaction-diffusion system, for the real and the imaginary parts of the order parameter. If the original reaction-diffusion system contains no cross-diffusion terms, but the self-diffusion terms are different, then the reduced reaction-diffusion system, corresponding to the CGLE, contains the full diffusion matrix including cross-diffusion term. Moreover, in that case the two eigenvalues of the diffusion matrix are complex. Incidentally, the two effective cross-diffusion coefficients will have signs opposite to each other, as in our Eq. (2).

Speaking of other possible analogies found in literature, in nonlinear optics there is a class of phenomena called "dissipative solitons," which also could be related to our quasisolitons. The literature on the topic is vast; we mention just one recent example [29]; for instance, compare Fig. 3 in that paper with our Fig. 13(a). Notice that the most popular class of models are variations of CGLE; e.g., models considered in Ref. [29] involve effective diffusion matrices precisly of the form (2).

Propagating pulses of complicated shape, resembling group quasisolitons, have also been observed in a model of blood clotting [30]. It is a three-component reaction-diffusion system, and "multihump" shapes are observed there for nonequal diffusion coefficients. A yet another possibility is the population dynamics with taxis of species or components onto each other, such as bacterial population waves; examples of nontrivial patterns there have been presented, e.g., in Refs. [10,31]. A spatially extended population dynamics model considered in Ref. [32] does not present complicated wave forms but is interesting as it demonstrates emergence of cross diffusion from a model with nonequal self-diffusion-only coefficients as a result of an asymptotic procedure. Finally we mention neural networks, where "antiphase wave patterns," resembling group quasisolitons, have been observed in networks of elements described by Morris-Lecar system [33]. The question whether all these resemblances are superficial, or there is some deeper mathematical connection behind some of them, presents an interesting topic for further investigations.

ACKNOWLEDGMENTS

M.A.T. was supported in part by Russian Foundation for Basic Research (RFBR) Grant No. 13-01-00333 (Russia). V.N.B. is grateful to A. Shilnikov and J. Sieber for bibliographic advice and inspiring discussions.

[1] A. G. Merzhanov and E. N. Rumanov, Rev. Mod. Phys. **71**, 1173 (1999).

[2] V. K. Vanag and I. R. Epstein, Phys. Chem. Chem. Phys. **11**, 897 (2009).

[3] O. V. Aslanidi and O. A. Mornev, J. Biol. Phys. **25**, 149 (1999).

[4] M. A. Tsyganov, J. Brindley, A. V. Holden, and V. N. Biktashev, Phys. Rev. Lett. **91**, 218102 (2003).

[5] V. N. Biktashev and M. A. Tsyganov, Proc. Roy. Soc. Lond. A **461**, 3711 (2005).

[6] V. N. Biktashev and M. A. Tsyganov, Phys. Rev. Lett. **107**, 134101 (2011).

[7] B. Malomed, in *Encyclopedia of Nonlinear Science*, edited by A. Scott (Routledge, New York, 2005), p. 639.

[8] J. H. E. Cartwright, E. Hernandez-Garcia, and O. Piro, Phys. Rev. Lett. **79**, 527 (1997).

[9] J. M. Chung and E. Peacock-López, Phys. Lett. A **371**, 41 (2007).

[10] M. A. Tsyganov, V. N. Biktashev, J. Brindley, A. V. Holden, and G. R. Ivanitsky, Physics-Uspekhi **50**, 263 (2007).

[11] J. D. Murray, *Mathematical Biology II: Spatial Modes and Biomedical Applications* (Springer, New York, 2003).

[12] M. A. Tsyganov, J. Brindley, A. V. Holden, and V. N. Biktashev, Physica D **197**, 18 (2004).

[13] I. Lengyel and I. R. Epstein, Science **251**, 650 (1991).

[14] See Supplemental Material at http://link.aps.org/supplemental/10.1103/PhysRevE.90.062912 for movies illustrating some of the figures.

[15] M. A. Tsyganov, V. N. Biktashev, and G. R. Ivanitsky, Biofizika **54**, 704 (2009) [Biophysics **54**, 513 (2009)].

[16] V. N. Biktashev, A. V. Holden, and E. V. Nikolaev, Int. J. Bifurcat. Chaos **6**, 2433 (1996).

[17] V. N. Biktashev and A. V. Holden, Physica D **116**, 342 (1998).

[18] P. Chossat, Acta Appl. Math. **70**, 71 (2002).

[19] A. J. Foulkes and V. N. Biktashev, Phys. Rev. E **81**, 046702 (2010).

[20] L. P. Shilnikov, Doklady Akademii Nauk SSSR **143**, 289 (1962) [Soviet Math. Dokl. **3**, 394 (1962)].

[21] L. P. Shilnikov, Mat. Sbornik **61**, 443 (1963), in Russian.

[22] S. H. Strogatz, *Nonlinear Dynamics and Chaos: With Applications to Physics, Biology, Chemistry, and Engineering* (Westview Press, Cambridge, MA, 2000).

[23] V. N. Biktashev, J. Brindley, A. V. Holden, and M. A. Tsyganov, Chaos **14**, 988 (2004).

[24] V. E. Zakharov and E. A. Kuznetsov, Zh. Éksp. Teor. Fiz. **113**, 1892 (1998) [J. Exp. Theor. Phys. **86**, 1035 (1998)].

[25] V. K. Vanag and I. R. Epstein, Phys. Rev. Lett. **88**, 088303 (2002).

[26] V. K. Vanag and I. R. Epstein, J. Chem. Phys. **121**, 890 (2004).

[27] N. Manz, B. T. Ginn, and O. Steinbock, Phys. Rev. E **73**, 066218 (2006).

[28] Y. Kuramoto, *Chemical Oscillations, Waves and Turbulence* (Springer, Berlin, 1984).

[29] D. A. Korobko, R. Gumenyuk, I. O. Zolotovskii, and O. G. Okhotnikov, Opt. Fiber Technol. **20**, 593 (2014).

[30] E. S. Lobanova and F. I. Ataullakhanov, Phys. Rev. Lett. **93**, 098303 (2004).

[31] M. A. Tsyganov, I. B. Kresteva, A. B. Medvinsky, and G. R. Ivanitsky, Doklady Akademii Nauk **333**, 532 (1993).

[32] Y. A. Kuznetsov, M. Antonovsky, V. N. Biktashev, and E. A. Aponina, J. Math. Biol. **32**, 219 (1994).

[33] A. S. Dmitrichev, V. I. Nekorkin, R. Behdad, S. Binczak, and J.-M. Bilbault, Eur. Phys. J. Special Topics **222**, 2633 (2013).